INTERNATIONAL JOURNAL FOR NUMERICAL METHODS IN FLUIDS, VOL. 8, 1543–1561 (1988)

DEVELOPING FLOWS IN NARROW CHANNELS, CONTAINING HEATED OBSTACLES

DENNIS TOROK AND ROSANNE GRONSETH

Corporate Research and Engineering, Control Data Corporation, 2800 East Old Shakopee Road, P. O. Box 1249, Minneapolis, Minnesota 55440, U.S.A.

SUMMARY

The use of numerical techniques to augment experimentally collected temperature data of electrical components is illustrated. FIDAP, a finite element CFD code, is used to generate the numerical results. Comparisons of the numerical results with experimental data of HaCohen, experimentally derived correlations of Wirtz and Dykshoorn and numerical results of Heaton *et al.* are given. A discussion of modelling techniques, mesh refinement, numerical error and stability is presented with suggestions for improvement of flow models. The results generated by FIDAP, using 2D models, compare favourably (to within 10%) with the experimental data of HaCohen. The results indicate the possibility of augmenting experimental data collection with numerical results, at least in the regions of laminar and low turbulent flow.

KEY WORDS Developing flow CFD FIDAP Finite element method Electronic packaging

INTRODUCTION

Hydrodynamic and thermal considerations are important in the design of computers, electrical circuit boards and peripheral equipment such as disc drives. Printed circuit boards (PCBs) are populated with electronic components or bare chips which generate heat. This heat must be removed through conductive, convective or radiative processes in order to keep the chip circuit junction temperature or component temperatures within acceptable levels to insure high levels of component reliability. The electronic components on the boards form arrays which may be symmetric or asymmetric. Cooling flow passes over, between and through channels formed by the packages. PCBs are usually stacked with air or other cooling media flowing through channels between the boards and around components providing the necessary convective cooling. Extensive experimental studies are usually made on prototype models of prospective designs to verify that the required board and component temperatures are maintained. It would be cost-effective in both time and resources if numerical means were available to augment experimentally obtained data in the early prototyping phase of the design process.

Velocity and thermal distributions in channels formed by stacked PCBs containing heated components are usually quite difficult to obtain without the use of sophisticated test equipment, i.e. hot wire and hot film anemometry or laser Doppler anemometry, and experienced personnel. Furthermore, because of the geometric scales of the components, it is difficult to obtain data on the velocity and thermal fields without disturbing the local fields themselves. Flow field visualization can be accomplished by use of smoke or trace materials injected into the fluid streams.[1–3] Prediction of component surface convective coefficients and ultimately the component tempera-

0271–2091/88/121543–19$09.50

Received 25 November 1987
Revised 25 April 1988

tures can be done indirectly, i.e. by evaporation of naphthalene-constructed components.[4] Knowing the amount of heat generation in a component through electrical measurements, embedding thermocouples, measuring free-stream or inlet temperature or calculating bulk temperature is also used to compute the average convective coefficient on the surface of a component in the channel. In general, as the components become smaller, the difficulty in obtaining accurate measurements increases.

Figure 1 illustrates the side and front views of an array of heated obstacles in a narrow channel. The subscript L denotes geometric characteristics in the longitudinal or flow direction, while the subscript T denotes geometric characteristics in the transverse or cross-flow direction. The effect of several geometric ratios on the flow field[5,6] can be developed from the geometry in Figure 1. The ratio of channel height to component height, H/B, characterizes the fraction of total flow around a component which affects the heat transfer. S_L/L_L characterizes the flow disturbance due to interaction of outer flow with cavity flow between two neighbouring components. S_L/B is associated with the separation, reattachment and redevelopment of boundary layer flows on individual components. The parameter S_T/L_T characterizes the amount of channelization which occurs between columns of components and therefore the three-dimensionality of the flow. Experimenters and numerical analysts[1,2,4-7] have studied arrays with 2D and 3D models using the above parameters in the range $1 < H/B < 5, 0{\cdot}25 < S_L/B < 12, 0 < S_L/L_L < 12$, which covers most of the actual board component packing densities currently in use. In most experimental studies the components are made of aluminium or copper.

The variation in the geometric parameters and measurement difficulties brought about by the small physical size of the component arrays under consideration lead one to investigate various means of augmenting experimental studies. The possibility of using numerical experimentation is being investigated in all areas of engineering. Computational fluid dynamics (CFD) is becoming an increasingly powerful tool in the aerodynamic design of aircraft and automobiles. The use of CFD in the aeronautics industry is well documented by Bradley.[8] Many of CFD's potential users are not yet aware of, or confident in, the use of low-speed, incompressible fluid flow codes to better understand engineering and manufacturing processes. The advantages of using numerical techniques to complement experimental testing are:

(1) the ability to investigate implications of design changes within relatively short time spans, resulting in increased design flexibility

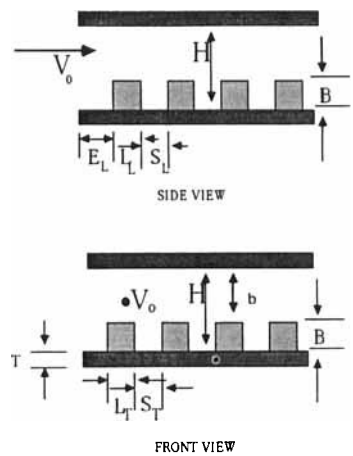

Figure 1. Developing flow in a narrow channel containing heated obstacles

(2) the capability of providing detailed information on all primitive variables, i.e. velocity components and temperature, throughout the physical domain
(3) the elimination of disturbances to the flow and thermal fields due to measurement devices
(4) the ability to simulate severe operating conditions
(5) the reduction in time and material costs
(6) the reduction in the range of conditions over which physical testing is required.

The capability of finite difference or finite element CFD codes to provide design and packaging engineers with an easily usable tool to visualize complex flow fields and evaluate thermal performance using various cooling scenarios has been illustrated by many investigators.[2, 9–14] Engelman,[14] however, warns of the danger of prematurely committing to the use of CFD codes in areas where the codes are unsuited or have not been verified against experimental data. In all cases one must evaluate CFD code capability in the particular area of interest by performing benchmark studies and comparing the numerical results obtained with the results obtained through experimental testing.[15–17] Only by establishing the code limits in particular engineering situations can a true confidence in the use of CFD codes be developed. The prediction of the flow and thermal fields in a channel containing heated obstacles has been selected as one initial problem for experimental comparison. FIDAP,[18] a commercial finite element code, has been selected for the initial comparative studies.

FORMULATION OF THE PROBLEM

Physical model

The physical system to be modelled was taken from the experimental study by HaCohen.[7] In this study the physical model was a 4×4 array of heated aluminium blocks mounted or embedded in a wood base. The dimensions of the blocks were 34 mm × 34 mm square with varying but equal array heights. The spacing between the array components was 14 mm both in the longitudinal (flow) and transverse (cross-flow) directions. The channel height was allowed to vary.

In the course of the experiments the channel height was varied from 2 to 15 mm and the component height was varied from zero (smooth channel) to 2 mm and to 4 mm. The component heat flux was varied up to 0·5 W cm^{-2} and the air velocity was varied up to 15 m s^{-1}. Power dissipation of each simulated flatpack, component, board and air temperatures, as well as channel static pressures, were measured at each run.

Figure 1 illustrates the model together with characteristic geometries. Two experimental cases of HaCohen were used for comparison with numerical results. Case 1, Run # 66, shown in Figure 2(A), had flush-mounted components and a channel height of 4 mm. Case 2, Run #27, shown in Figure 2(B), had channel blocks of height 2 mm. The approach velocity was 6·93 m s^{-1} for Case 1 and 6·71 m s^{-1} for Case 2. The base of the channel was plywood 2·5 mm thick. Table I summarizes the geometric ratios and Reynolds numbers for the comparative runs of HaCohen.[7]

Field equations and boundary conditions

The derivation of the finite element method (FEM) will not be developed here; application of the FEM to the solution of the field equations in fluid dynamics has been described in the FIDAP theoretical manual.[18] The continuity, momentum and energy equations for developing flow of a fluid in a channel are given in dimensionless form as

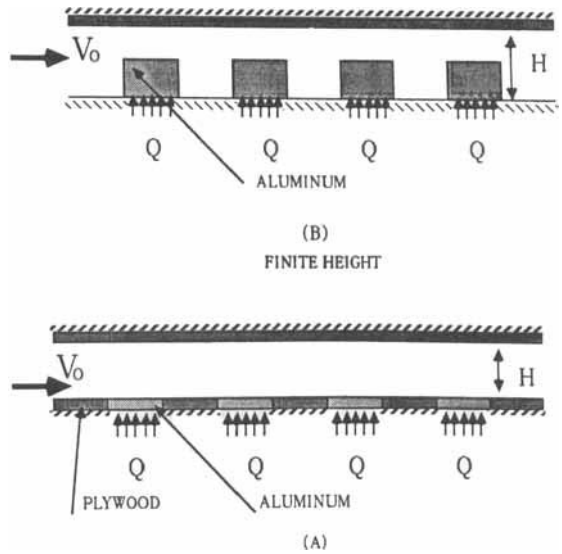

Figure 2. Thermal loadings for flush-mounted and finite height components

Table I. Experimental models

Study (Figure 1)	HaCohen[7] Run # 66 Case 1 (Figure 2(a))	HaCohen[7] Run # 27 Case 2 (Figure 2(b))
B/H	0	0·5
L_L/L_T	1	1
S_L/S_T	1	1
$(S/L)_L$	0·412	0·412
B/L_L	0	0·143
H/L_L	0·12	0·12
S_L/L_L	0·41	0·41
B(mm)	0	2
L_L(mm)	34	34
L_T(mm)	34	34
S_L(mm)	14	14
S_T(mm)	14	14
H (mm)	4	4
E_L (mm)	2·5	2·5
Q (W)	3·375	3.59
V_0 (m s^{-1})	6·91	6·71
$Re\,(L_L)$	1·57E + 04	1·54E + 04
$Re\,(2H)$	3703 at $T_{in} = 19{\cdot}5\,^{\circ}C$	3622 at $T_{in} = 18\,^{\circ}C$

$$\nabla \cdot \mathbf{U} = 0, \tag{1}$$

$$\mathbf{U} \cdot \nabla \mathbf{U} = -\nabla P + \frac{1}{Re} \nabla^2 \mathbf{U}, \tag{2}$$

$$\mathbf{U} \cdot \nabla T = \frac{1}{P_e} \nabla^2 T, \tag{3}$$

with the dimensionless variables given as

$$\mathbf{U} = \frac{\tilde{\mathbf{U}}}{V_0}, \qquad X = \frac{\tilde{x}}{D_h}, \qquad T = \frac{\tilde{T} - T_{\text{in}}}{\Delta T_{\text{ref}}}, \qquad P = \frac{\tilde{P}}{\rho V_0^2},$$

$$P_r = \frac{\mu}{\alpha}, \qquad R_e = \frac{V_0 D_h}{\mu}, \quad P_e = R_e P_r.$$

It is ultimately the control of temperature in the solid that is important, and therefore the coupling of the conduction in the packages and the convection heat transfer in the fluid should be considered simultaneously. If the conduction in the solid is not included, then the usual thermal boundary conditions are either uniform temperature or uniform heat flux, which approximates a highly conductive or a low-conductivity solid region respectively. If the conjugate problem is analysed—that is, the analysis includes the simultaneous solution of the hydrodynamic and energy equations for the fluid and solid regions—then the energy equations for these solid regions must be included:

$$\frac{1}{P_e} \frac{k_i}{k_{\text{air}}} \nabla^2 T = 0. \tag{4}$$

In equation (4) $i = 1$ and $i = 2$ denote the component and channel wall materials respectively.

The thermal boundary condition best suited for the model describing the physical geometry of HaCohen[7] is a heat flux boundary at the base of the components as illustrated in Figures 2(a) and 2(b). HaCohen's geometry consisted of a duplicate array of heated blocks situated back-to-back with heating elements at the interface. This insured that no heat loss would occur through the base. In the current analysis it was also assumed that the contact resistance between the components and the base was negligible. The dimensionless heat flux used in the numerical study was defined as

$$q = \frac{Q}{Re\, Pr\, q_{\text{ref}}\, L_{\text{L}}\, W}, \tag{5}$$

where

$$q_{\text{ref}} = \frac{k}{D_h} \nabla T_{\text{ref}}.$$

The reference temperature difference is arbitrary and has been taken as unity for simplicity.

While the physical model is three-dimensional, the problem currently being solved is taken as 2D. The width of the block is less than the pitch of the array in the transverse direction. However, to insure correct heat input in the 2D analysis, the heat flux is calculated assuming a uniform heat flux in the transverse direction based on the pitch $W = L_{\text{T}} + S_{\text{T}}$ of the array. This insures that the correct sensible heating of the air occurs in the flow tube with cross-section $H \times W$. The remainder of the base and the top wall of the channel have adiabatic boundaries. All solid surfaces are assumed to be zero-slip and zero-throughflow boundaries. At the channel inlet the velocity is

taken as uniform and parallel to the channel walls with a magnitude of unity for developing flow. A parabolic flow with a maximum dimensionless centreline velocity of $V_{in} = 1{\cdot}5$ can also be applied. The dimensionless temperature of the fluid is taken as zero at the inlet. For the geometry under consideration the component pitches in both the flow and cross-flow directions are equal. The ratio of channel height to component length is $H/L_L = 0{\cdot}12$ and the ratio of spacing between components to component length is $S_L/L_L = 0{\cdot}41$. Asako and Faghri[13] presented numerical results of a 3D analysis of rectangular blocks in a fully developed channel flow. They also presented studies on the applicability of 2D models for the same geometries. They found that for ratios of spacings as defined above, the component Nusselt number predicted by a 2D analysis was approximately 5–10% lower than obtained from a 3D analysis of the same geometry. It would be expected that the components modelled in this 2D analysis would have temperatures slightly higher, perhaps 1–1·5°C, than found in an equivalent 3D analysis if the same convective surface area was used. All analyses were performed using FIDAP on a CDC 910 workstation, running under UNIX, with dual hard discs totalling 250 MB. 3D computations of multiple components in the array would require significantly larger computational resources and therefore could not be run effectively in the current environment.

Mesh generation

FIDAP includes a mesh generator, FIMESH, which utilizes a mapping procedure between a logical plane and a geometric space. It uses an indexing scheme to number boundaries, surfaces and regions and to control the generation of nodal points, elements and mesh grading and the application of boundary conditions. The logic space and the geometric space for the region under consideration are shown in Figure 3. The initial description of the logical indices I and J will allow

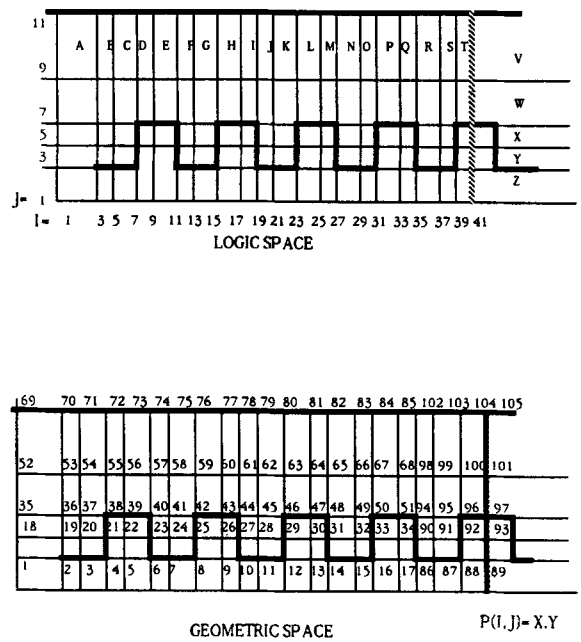

Figure 3. Generic model of channel mesh

the gradation of the mesh at each of the solid–fluid boundaries. The difference between any two I or J indices specifies the number of elements within that region. By use of an index expansion parameter, the I and J can be expanded without modification of the logical and geometric spaces. This capability in FIDAP allows the set-up of a generic model for the region including the channel, solid components and, if required, the substrate. Since the model discretization requirements for a given level of accuracy are not known *a priori*, the ability to modify grid density and gradation quickly is useful. This generic model was used for both the flush-mounted devices and those of finite height.

Table II indicates the various mesh discretizations which have been utilized in the development of the channel flow models. Each sector of the model, labelled A to T, is discretized with the number of elements as shown in Table II. The model was developed utilizing the parametric expansion features in FIDAP, and it is therefore relatively simple to append the baseline fluid model to include the coupled problem of the fluid, component and base.

The solution accuracy and numerical stability of the solution procedure are sensitive to the dimensions of the elements in the regions where both the flow field and the thermal field are rapidly changing in magnitude and/or direction. The grid Peclet number is seen as the critical parameter in determining the numerical stability of the solution procedure. A grid Peclet number $Pe > 2$ coupled with large streamwise gradients in the advected direction usually gives rise to 'wiggles' in the computed velocity field as discussed by Gresho and Lee.[19] As long as the grid is sufficiently small in the critical regions of the flow, i.e. across the component surfaces, then 'wiggles' in the computed velocity and thermal fields, in regions removed from these critical areas, may still yield acceptable solutions. Higher values of the grid Peclet number could also cause temperatures in isolated regions to be lower than the minimum inlet temperature. Attempting to keep the grid Peclet number below the critical value may require an excessively large number of

Table II. Mesh discretization for the various models

	Element density in regions A–P in flow direction																			
Model	A	B	C	D	E	F	G	H	I	J	K	L	M	N	O	P	Q	R	S	T
$B/H = 0$																				
G	2	6	17	10	5	6	12	8	4	6	12	8	4	6	12	6	—	—	—	—
I	2	6	17	10	5	6	12	8	4	6	12	8	4	6	12	6	—	—	—	—
$B/H = 0{\cdot}5$																				
D	2	6	17	10	5	6	12	8	4	6	12	8	4	6	12	6	—	—	—	—
F	2	10	30	15	15	10	10	10	—	—	—	—	—	—	—	—	—	—	—	—
K	2	6	17	10	5	6	12	8	4	6	12	8	4	6	12	8	4	6	12	6

	Element density in regions V–Z in y-direction				
Model	V	W	X	Y	Z
$B/H = 0$					
G	7	7	8	7	4
I	4	3	10	10	6
$B/H = 0{\cdot}5$					
D	7	7	8	7	—
F	10	14	8	7	—
K	7	12	5	5	—

elements. In the analysis presented here, isolated regions of temperatures lower than the inlet do occur. These may be allowable as long as they are in regions removed from the heat-generating surfaces and if the results of the analysis are acceptable from an engineering point of view. Table III indicates the model size, bandwidth and element minimum dimensions in the vicinity of the components for all models included in this analysis.

Model D was the initial coarse grid model for a 2D analysis of a 4 × 4 component array. Model K had a finer grading near the obstacles both in the flow direction and in the channel height direction. Model F had a still finer grading of elements for the first component in the row of the array. The element dimensions were made non-dimensional with respect to the channel hydraulic radius $2H$. Models G and I were developed for flush-mounted components and include the substrate region. Model I is similar to model G, with the total number of elements in the 'y'-direction being the same, but with an increased element mesh density near the channel base.

SOLUTION PROCEDURE

The non-dimensionalized field equations describing the flow are highly non-linear, and therefore it is usually the case that a solution at a particular load step, i.e flow Reynolds number and component heat flux, be obtained by stepping through several intermediate solutions. The intermediate loadings are given in Table IV. The solutions at these load cases are used as initial iterates for the thermal and fluid flow field for the solution at the next load step. In the present

Table III. Model characteristics and minimum element dimensions ($X/2H$)

Model	Nodes	Elements	BW	Element dx	Element dy
$B/H = 0$					
G	4182	4026	116	0·021	0·0041
I	4182	4026	116	0·021	0·0010
$B/H = 0{\cdot}5$					
D	3690	3538	103	0·021	0·0042
F	4040	3900	123	0·0005	0·0004
K	4590	4408	103	0·0009	0·0026

Table IV. Dimensionless loading parameters

Reynolds number	Heat dissipation $B/H = 0$ 3·375 W	Heat dissipation $B/H = 0{\cdot}5$ 3·59 W	Viscosity	Conductivity Air	Conductivity Al	Conductivity Wood
500	1·7950	1·9093	0·002	0·002821	22·073	0·01033
1000	0·89748	0·95465	0·001	0·001210	11·036	0·00517
2000	0·44874	0·47733	0·0005	0·000705	5·518	0·00258
3000	0·29916	0·31822	0·000333	0·000470	3·679	0·00172
3500	0·25642	0·27276	0·0002857	0·000403	3·153	0·00148
3622	0·24778	0·2685	0·0002761	0·000389	3·126	0·00147
3703	0·24620	0·26263	0·0002701	0·000381	3·051	0·00143
4000	0·22437	0·23866	0·00025	0·000353	2·759	0·00129

study the channel Reynolds number was calculated to be $Re = 3622$ at $T_{in} = 18°C$ for the case where $B/H = 0{\cdot}5$ (HaCohen data set # 27) and $Re = 3703$ at $T_{in} = 19{\cdot}5°C$ for the case where $B/H = 0$ (HaCohen data set # 66). Solutions were obtained at $Re = 500$, 1000, 2000 and 3000 before the solutions for $Re = 3622$ and $Re = 3703$ were attempted. Table IV summarizes the loading parameters for both cases.

The property values for air at 18°C and 19·5°C as well as the conductivities of aluminium, ceramic and plywood are given in Table V.

Since the field equations were solved in dimensionless form, temperature dependency when required was supplied through a dimensionless viscosity $1/Re$ and a dimensionless conductivity $1/Pe$. All property effects were combined in these terms. In dimensionless form the heat flux was found to be temperature-independent. Table VI illustrates the variability of the dimensionless parameters as a function of temperature.

Table V. Material properties

Air	18°C	19·5°C
Density (kg m^{-3})	1·216	1·209
Specific heat (J kg^{-1} K^{-1})	1004·5	1004·7
Conductivity (Watts m^{-1} K^{-1})	0·0255	0·0256
Viscosity (Pa s)	1·802E−05	1·810E−05
Aluminium		
Conductivity	205 W m^{-1} K^{-1}	
Ceramic		
Conductivity	20·5 W m^{-1} K^{-1}	
Plywood		
Conductivity	0·096 W m^{-1} K^{-1}	

Table VI. Temperature dependence of dimensionless parameters

(a) Flow Reynolds number $Rey = 3703$ at 19·5°C, $B/H = 0$

Temperature (°C)	$\mu = 1/Re$	$K_1 = 1/Pe_1$	K_2(A1)	K_3 (wood)
2	0·0002436	0·0003417	2·8827	0·001350
19·5	0·0002701	0·0003810	3·0510	0·001429
27	0·0002844	0·0004023	3·1478	0·001474
52	0·0003276	0·0004673	3·3973	0·001591
77	0·0003729	0·0005350	3·6558	0·001712
102	0·0004203	0·0006073	3·9027	0·001828

(b) Flow Reynolds number $Rey = 3622$ at 18°C, $B/H = 0{\cdot}5$

Temperature (°C)	$\mu = 1/Re$	$K_1 = 1/Pe_1$	K_2 (A1)	K_2 (ceramic)
2	0·0002503	0·0003511	2·9620	0·29620
18	0·0002761	0·0003887	3·1248	0·31248
27	0·0002922	0·0004133	3·2338	0·32338
52	0·0003366	0·0004802	3·4958	0·34958
77	0·0003831	0·0005496	3·7556	0·37556
102	0·0004318	0·0006240	4·0100	0·40100

The usual solution approach when incorporating temperature-dependent properties was to first obtain the solution based on constant properties evaluated at the inlet temperature and then perform an additional load step iteration to a converged solution using temperature-dependent parameters.

Two geometric models were analysed. Case 1 had flush-mounted components embedded in the plywood channel base ($B/H = 0$), while Case 2 had finite height components ($B/H = 0{\cdot}5$). Both cases were compared to the experimental results of HaCohen,[7] Case 1 with data set # 66 and Case 2 with data set # 27. Representative execution times for one iteration are given in Table VII.

Approximately 10–20 iterations were usually required to obtain convergence at any load step. Convergence was assumed when the solution at the $(i+1)$th iteration was within 1% of the solution at the ith iteration. The solution procedure employed in the analysis was to start each load step with 3–5 iterations of successive substitution followed by 5–15 additional iterations of a quasi-Newton method with matrix updating. An explanation of these methods is given in the FIDAP theoretical manual.[18] For example, to obtain convergence at the first load step of model D, $Re = 500$, 10 iterations were required for a total of approximately 2·6 h. Four additional intermediate load steps, i.e. $Re = 1000$, 2000 and 3000 plus the final design point Reynolds number, required approximately 11 additional hours. One could obtain a particular Reynolds number solution, $Re = 3622$ for instance, in 2–3 days turnaround, executing in the background mode in a workstation environment. It should be noted that while these runs were being made in the background mode, additional post-processing of previous results or the generation of new models could be processed interactively.

RESULTS

Flow and thermal field visualization

The capability of rapidly viewing the flow and thermal fields during the analysis is a distinct advantage when performing CFD calculations. Figure 4 is a superposition of the four components, the upper left being the entrance to the channel and the lower right being the channel exit. It illustrates the developing velocity fields using the mesh for model K. For the given array geometry and inlet flow conditions, the velocity field in the gap between the channel and the first and second component is seen to be developing. By the fourth component, however, the flow field in the gap is almost fully developed. This is clearly shown in Figure 5, which plots superimposed velocity profiles at channel cross-sections at the mid-length of each component. The average velocity at the inlet is taken as unity in the system of dimensionless variables used in the analysis. However, in the region of the channel above each of the components, the integrated value of the dimensionless

Table VII. Workstation execution times

Model	*BW*	Nodes	Elements	Equations	Solution time (one iteration) (min)
D	103	3690	3538	9027	15·8
F	103	4590	4408	11837	21·2
K	133	4040	3900	10349	27·1
G, I	114	4182	4408	10498	20·5

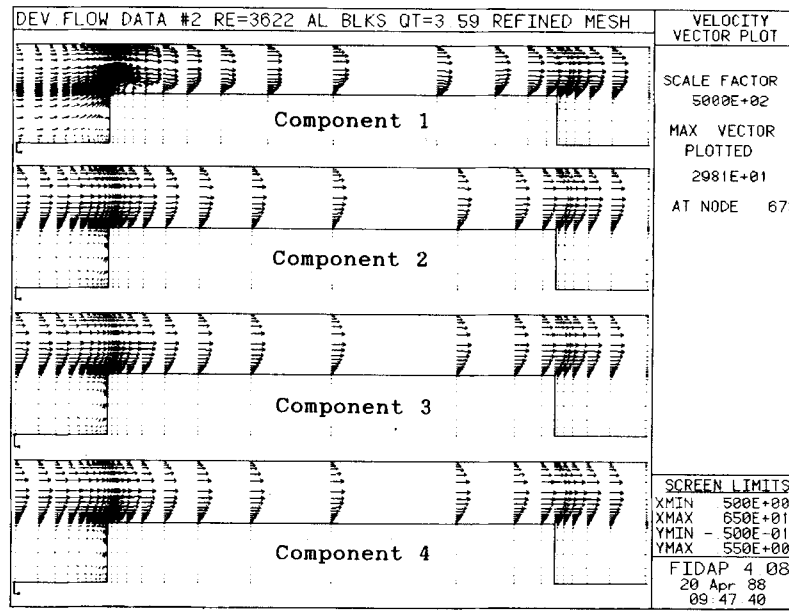

Figure 4. Velocity vector field over components

velocity is twice that of the inlet since the area ratio is half that at the inlet. The ordinant in Figure 5 describes the dimensionless velocity. For fully developed flow the ratio of the channel centreline velocity to the average channel velocity (inlet velocity) is 1·5; therefore for fully developed flow in the gap between the channel and the component, a fully developed centreline velocity should have a value of three times the average inlet velocity. From Figure 5 the flow is

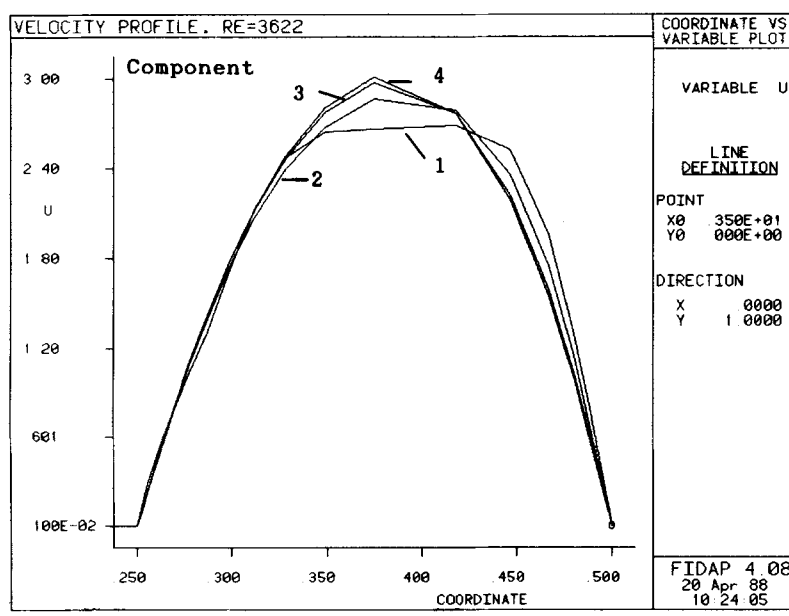

Figure 5. Velocity profiles at centre of each component illustrating flow development

seen to be almost parabolic by the fourth component, with a ratio of centreline velocity to channel inlet velocity of 3.

Figure 4 shows a small separated region just downstream of the leading edge of the first component. This region is illustrated more clearly in Figure 6 using the more refined mesh of model F. The separated flow reattaches to the component approximately one-tenth of the component length downstream. Figure 7 shows the streamlines of the flow around the first component and clearly indicates the formation of the separated flow region.

Figure 8 illustrates the isotherms above each component. One can see that, in a large percentage of the channel gap, the fluid in the channel is near the channel inlet temperature and is influenced only slightly by the presence of the heat-generating components. Figure 9 is a line plot superimposing, for several channel elevations above the components, channel temperatures in the flow direction. The temperatures of the components, signified by the uppermost curve, are seen to be quite uniform because of their high thermal conductivity. The lower curve, signifying the fluid temperature near the channel upper wall, experiences only a slight temperature increase. As the ratio of component height to channel height increases, it is expected that the heated obstacles will influence the channel temperature to a greater degree. For the same velocity field the effect of component thermal conductivity is illustrated in Figure 10, which is analogous to Figure 9 except the conductivity of the components is taken to be one-tenth of that of aluminium. This is approximately in the range of many of the ceramic materials currently being used in chip carriers. While the variation of aluminium component temperature was less than 1 °C, the ceramic

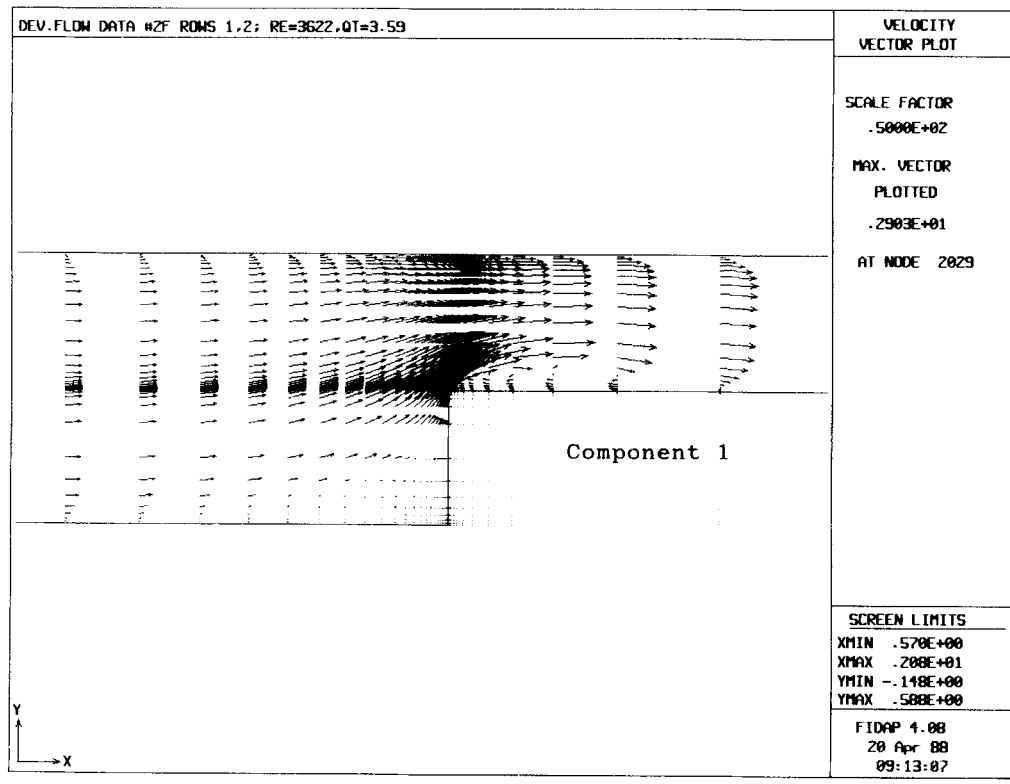

Figure 6. Separated flow at upstream corner of first component

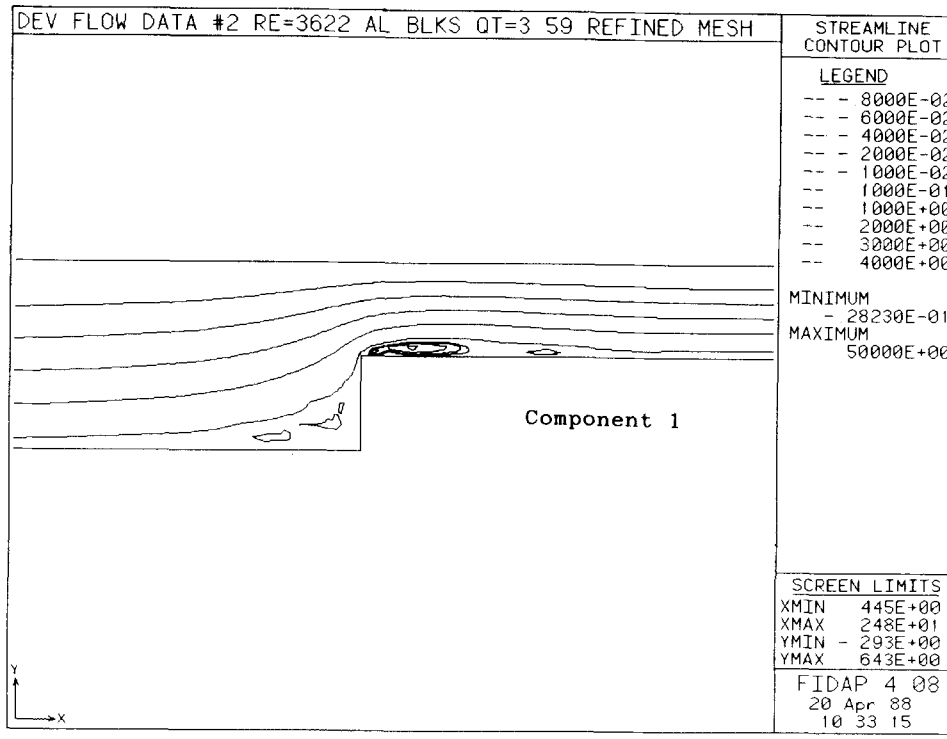

Figure 7. Streamlines across first component

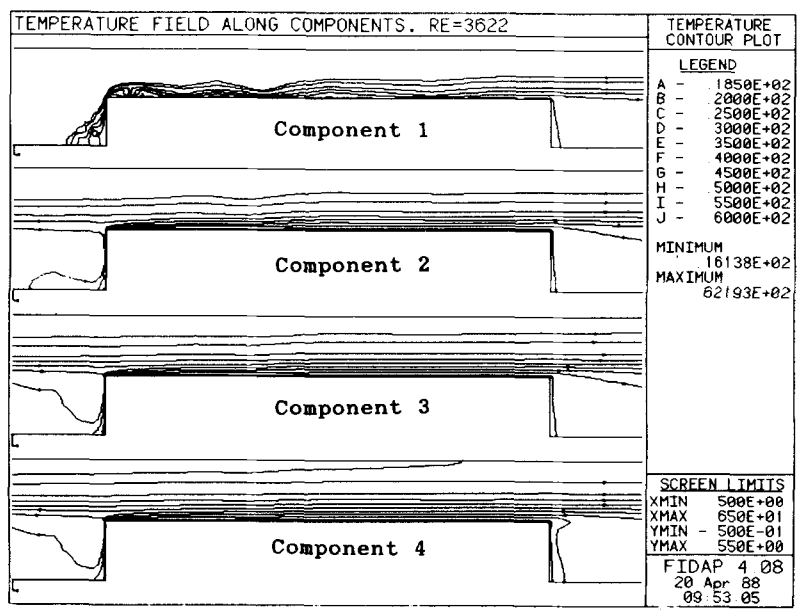

Figure 8. Contours of developing temperature field in channel line plots

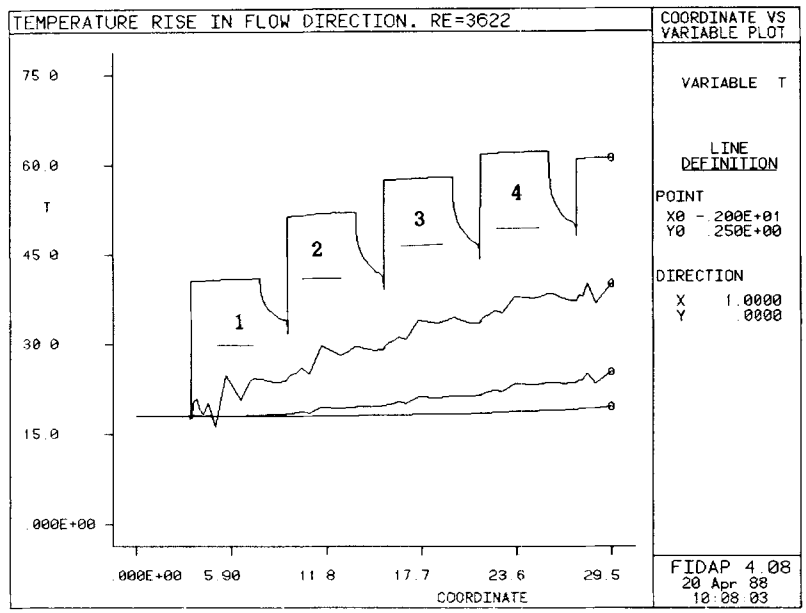

Figure 9. Fluid temperature rise in flow direction for aluminium components

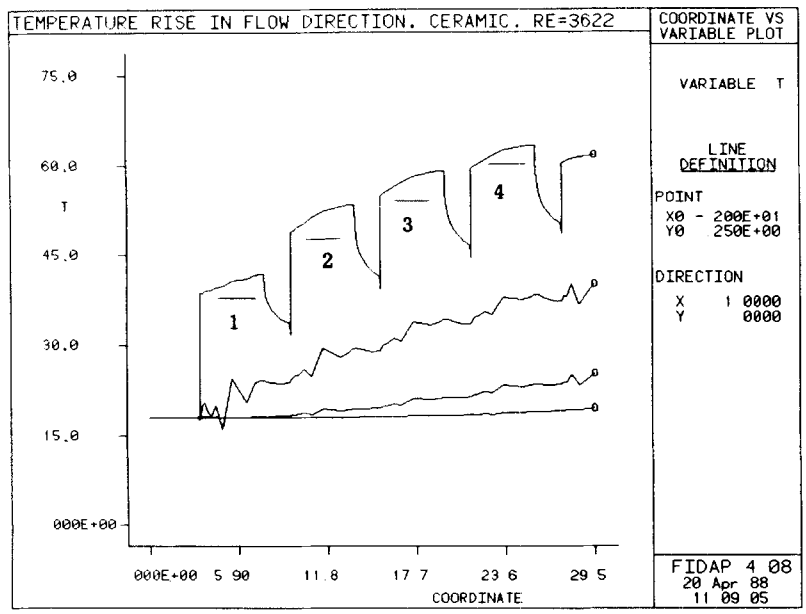

Figure 10. Fluid temperature rise in flow direction for ceramic components ($K_c/K_a = 0{\cdot}1$)

components increase by 4–5°C along the surface from their upstream and downstream edges. Actual chip carriers will experience much greater variations in temperature.

The inadequacy of the mesh to resolve the flow gradients upstream of the first component is illustrated in Figures 9 and 10. They show isolated regions, near the inlet and upstream of the first

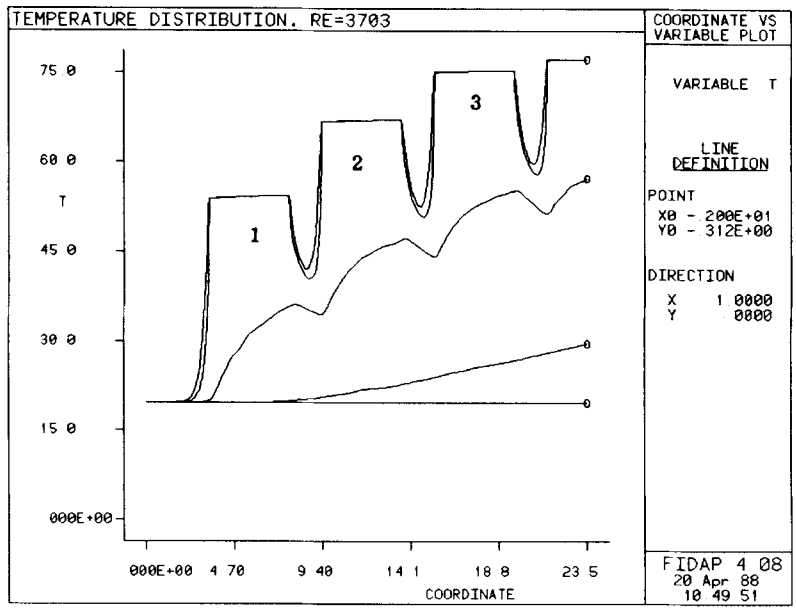

Figure 11. Temperature rise in fluid and base in flow direction for flush-mounted components

component, where the local temperature is less than the inlet temperature, $T_{in} = 19{\cdot}5\,^{\circ}C$ for Case 1 and 18 °C for Case 2. The grid Peclet number in this region was calculated to be in the range 30–40. For model K the minimum temperature, found just upstream of the first component in the region of highest velocity gradients, was 16·13 °C. After additional mesh refinement in this region, model F, the minimum temperature in the same region was found to be 17·1 °C. Further refinement of the mesh can be expected to reduce this temperature excursion.[19] Changing the inlet velocity to a parabolic profile did not significantly improve the temperature field in this region. Increasing the inlet length was not investigated, but it is expected that the inadequacy of the mesh to resolve the temperature field slightly upstream of the first component will still be present. With the current meshes, the numerical inaccuracies influenced the temperature level of the first component, as will be seen in the comparisons with experimental data.

The temperature rise in the channel at several elevations above the flush-mounted components is shown in Figure 11. This model included only the first three components and half of the fourth. Fully developed flow was present by the third component. Much of the channel again remains at or close to the inlet temperature of 19·5 °C. The five curves from bottom to top in Figure 11 show the temperatures at the channel centreline, at a quarter of the distance to the base, at half the distance to the base, at the surface of the base and at the outer channel wall. Since there are no high flow gradients caused by flow acceleration, decelaration and directional changes, no suppression of the temperature field in the vicinity of the first component is seen.

Comparison with experimental data

Component temperatures ($B/H = 0$). Flush-mounted components were analysed and compared with data set # 66 from HaCohen.[7] In this model the channel base was included in the analysis using models G and I. These models were also run with temperature-dependent properties, signified by G(T) and I(T). Model I had mesh refinement in the y-direction for elements

near the channel base, a factor of four finer than model G. Table VIII illustrates the results of the comparison with experimental data. Heaton *et al.*[20] provide numerical results of Nusselt numbers for developing flow and temperature in a channel with one wall having uniform heat flux and the other wall adiabatic. Their results, using local wall minus mixed fluid temperature as the driving potential, yield lower results than the numerical results of FIDAP. Results from Heaton's data were calculated using an area-weighted average wall heat flux computed using the discrete source data of HaCohen.

The temperatures given in Table VIII reflect the component surface temperature and channel surface temperature in the regions between components. Models G and I have the same number of elements in the y-direction; however, the size of the first element at the channel surface for model I is a factor of four finer than that for model G.

The component temperatures given in model I(T) are seen to agree rather well with the experimental data of HaCohen. Comparing models G, G(T) and I(T), mesh refinement has a somewhat greater effect on component temperatures than that due to a temperature-dependent variation in fluid properties, at least for the mesh refinements attempted in this study. However, it is apparent that both effects should be considered when doing analyses.

Component temperatures ($B/H = 0{\cdot}5$) The component temperature range for heat-generating obstacles with $B/H = 0{\cdot}5$ and a flow Reynolds number of 3622 is given in Table IX, which also includes the experimental results of HaCohen (Run # 27) and predictions based on the empirical formulation of Wirtz and Dykshoorn.[21]

For the numerical models designated by D, K and K(T) an execution run was made with a velocity profile, designated by 'U', and a parabolic profile, denoted by 'P', as the inlet velocity boundary conditions. As seen in Table IX, when comparing the results for uniform and parabolic inlet boundary conditions, there is little difference found in the component temperatures. The results indicate numerically predicted component temperatures agree to within 11% of experimental data. The poorest agreement is with the first element; this is attributed to the grid Peclet number as described by Gresho and Lee.[19] In addition, model D does not include the region downstream of the last (fourth) component. This was done initially to reduce the size of the model on a workstation. In order to accurately include all the recirculation zones downstream of the last component, which is in fact the region downstream of a backward-facing step, sufficient elements

Table VIII. Average component temperatures (°C); $B/H = 0$, flow Reynolds number $Re = 3535$ at $T_{in} = 19{\cdot}5$°C

Component	Experimental	Numerical models G	G(T)	I(T)(%)	Correlation Heaton[20]
1	53·5	56·1	54·8	54·0 (0·9%)	49·2
Between channel	1–2				
	31·1	41·8	41·3	40·5	
2	62·1	71·1	68·2	66·8 (7·6%)	61·9
Between channel	2–3				
	37·3	52·8	52·4	50·9	
3	67·6	81·1	76·8	75·1 (11·1%)	66·1
Between channel	3–4				
	40·1	61·0	60·1	57·9	
4	74·9	83·8	78·9	77·1	68·0
Between channel	4–				
	29·2	—	—	—	

Table IX. Component temperature ranges (°C); $B/H = 0{\cdot}5$, flow Reynolds number $Re = 3622$ at $T_{in} = 18$°C

Component number / Inlet boundary		Experiment HaCohen[7] Run # 27	Numerical models D	K	K(T)	F(T)	Correlation Wirtz[21]
1	U	47·7	39·3	41·7	40·7	42·2 (−11·5%)	47·8
	P		39·2		39·9		
2	U	53·5	51·4	54·0	51·7 (−3·3%)	—	50·0
	P		51·8		51·4		
3	U	56·8	58·6	60·8	57·3 (1·4%)	—	51·5
	P		58·0		57·4		
4	U	61·4	55·2	65·9	61·6 (0·8%)	—	52·7
	P		54·9		61·7		

must be included such that the boundary conditions at the exit do not include any inflow regions.This would make the model excessively large. Therefore the exit boundary of the model was taken at the midline of the fourth component. It was assumed that the thermal boundary was adiabtic, which meant that equal heat would flow out of the component through the fore and aft section. Since the rear portion of the component generally has poorer heat transfer characteristics, this assumption would tend to suppress the temperature level of the fourth component as seen in Table IX. Comparison of predicted temperatures of the fourth component with experimental data is better with model K(T) than with model D. Model K(T) includes temperature-dependent properties and a complete fourth component and is within 1% of the experimental values obtained by HaCohen.[7] Refining the mesh in both the flow and vertical direction, model F(T), improves the comparison of the temperature of the first component with that obtained by experiment. The refined mesh of model F also decreased the local temperature excursion, due to numerical inaccuracies caused by a greater than critical grid Peclet number, to less than 1°C. Since the temperature levels of the second and third components had satisfactory agreement with experimental data, model F contained only the first component plus the fore section of the second component. Better results would be anticipated if the second and third components were also modelled using the mesh of model F. This was not done at this time because of resource limitations in the workstation environment. The channel base was not included in the case where $B/H = 0{\cdot}5$. The results of Wirtz and Dykshoorn[21] are given in the last column of Table IX. Their correlation, which is applicable to 3D arrays in the fully developed flow region, yields results which predict component surface temperatures lower than those obtained by HaCohen using his flow and geometric conditions. The ratio of top surface to total surface area is 0·68 for HaCohen's geometry, while Wirtz and Dykshoorn state the applicability of their formulations to area ratios greater than 0·5. In addition, the ratio of spacing between components to component length, B/L_L, is significantly larger in Wirtz and Dykshoorn's component array than for HaCohen.[7]

In the flush-mounted case the temperatures of the downstream components tended to be somewhat elevated when compared with experimental values. One possible reason is that localized turbulence may be occurring. The laminar conductivity of the fluid is lower than the effective turbulent conductivity, resulting in a somewhat lower heat removal capability, and therefore the predicted component temperatures would be expected to be higher for laminar flow than for turbulent flow. Further studies will be initiated using turbulent models to predict

temperature fields. In any case, Reynolds numbers between 3000 and 4000 seem to be the upper limit for the laminar models to obtain results to a reasonable engineering accuracy (to within 10% when compared to experimental data).

CONCLUSIONS

When executing FE codes on individual workstations, it is necessary to balance the added computational time necessary when going to a refined mesh against the potential benefits of increased accuracy. Workstations are advantageous when initially prototyping a new model and developing a solution procedure. Finite element codes for the determination of thermal and fluid flow fields in electronic components have been shown to offer an acceptable alternative to early experimental studies on prototype models. It is anticipated that with careful mesh development, accuracies to within 10% or better can be achieved when compared to experimental data. Since 2D models are presently being used in numerical studies to simulate 3D flow fields, it is unlikely that further grid refinement would be cost-effective in the present environment.

Further studies should be initiated to evaluate the flow fields in arrays using 3-D models and turbulence models. A comparison of k–ε models and mixing length models for channel flows would be informative. CFD codes provide a useful tool to assist the design engineer in developing cooling techniques for microelectronic components. Numerical techniques can currently provide accurate qualitative predictions for flow and thermal field visualization. Further studies are needed on 3D effects, turbulence models and transient effects to increase the accuracy of quantitative results.

APPENDIX: NOMENCLATURE

α	fluid diffusivity ($m^2\,s^{-1}$)
B	height of component (mm)
C_p	specific heat ($J\,kg^{-1}\,K^{-1}$)
D_h	channel hydraulic diameter (mm)
H	channel spacing (mm)
k	fluid conductivity ($W^{-1}\,m^{-1}\,K^{-1}$)
L	component length characteristic (mm)
μ	fluid viscosity ($m^2\,s^{-1}$)
$\tilde{P}$	pressure ($N\,m^{-2}$)
Pe	Peclet number, $Pe = Re\,Pr$
Pr	Prandtl number, $Pr = \mu/\alpha$
q_{ref}	component reference heat flux ($W\,m^{-2}$)
q^*	dimensionless heat flux
Q	component power W
ρ	fluid density ($kg\,m^{-3}$)
Re	channel Reynolds number, $Re = V_0 D_h/\mu$
S	spacing between components (mm)
$\tilde{T}$	temperature (K)
ΔT_{ref}	reference temperature difference (°C)
$\tilde{U}_i$	velocity component in co-ordinate direction
V_0	channel inlet velocity ($m\,s^{-1}$)
W	pitch of components in cross-stream direction (mm)

REFERENCES

1. G. L. Lehmann and R. A. Wirtz, 'Effect of variations in streamwise spacing and length on convection from surface mounted rectangular components', *HTD-48, 23rd National Heat Transfer Conf.*, Denver, CO, August 1985, pp. 39–47.
2. D. E. Arvizu and R. J. Moffat, 'The use of superposition in calculating cooling requirements for circuit board mounted electronic components', *IEEE Paper CH1781-4/48-0133* (1982).
3. N. Ashiwake, W. Nakayama and T. Daikoku, 'Forced convection heat transfer from LSI packages in an air-cooled wiring card array', *HTD-28, ASME Winter Annual Meeting*, Boston, MA., November 1983, pp. 35–42.
4. E. M. Sparrow, J. E. Neithammer and A. Chaboki, 'Heat transfer and pressure drop characteristics of arrays of rectangular modules encountered in electronic equipment', *Int. J. Heat Mass Transfer*, **25**, 469–473 (1982).
5. R. J. Moffat, D. E. Arvizu and A. Ortega, 'Cooling electronic components: forced convection experiments with an air cooled array', *Heat Transfer in Electronic Equipment, ASME HTD-48.*, 1985, pp. 17–27.
6. M. J. Chang, R. J. Shyu and L. J. Fang, 'An experimental study of heat transfer on mounted components to a channel airflow', *ASME Preprint 87-HT-75, National Heat Transfer Conf.*, Pittsburgh, PA, 1987.
7. Y. HaCohen, 'Convective heat transfer coefficients for elements on a packed board', *M.Sc. Thesis*, Ben-Gurion University of the Negev, 1985
8. R. G. Bradley (ed.), *Current Capabilities and Future Directions in Computational Fluid Dynamics*, National Academy of Sciences and National Research Council, Washington, DC, 1986.
9. R. H. Pletcher and S. V. Patankar, 'Computers in analysis and design', *Mech. Eng.*, **105**, 73–79 (June 1983).
10. S. V. Patankar and M. E. Braaten, 'Analysis of laminar mixed convection in shrouded arrays of heated rectangular blocks', *ASME HTD-32, National Heat Transfer Conf.*, Niagara Falls, NY, August 1984, pp. 77–84.
11. D. F. Torok, 'Augmenting experimental methods for flow visualization and thermal performance prediction in electronic packaging using finite elements', *HTD-32, ASME Heat Transfer Conf.*, Niagara Falls, NY, August 1984, pp. 49–57.
12. A. T. Patera, 'A spectral element method for fluid dynamics', *J. Comput. Phys.*, **54**, 468 (1984).
13. Y. Asako and M. Faghri, 'Three dimensional heat transfer and fluid flow analysis of arrays of rectangular blocks encountered in electronic equipment', *ASME Preprint 87-HT-73, National Heat Transfer Conf.*, Pittsburgh, 1987.
14. M. Engelman, 'Computational fluid dynamics: pouring it on too thick?', *Comput. Mech. Eng.*, **6**, 52–56 (January 1987).
15. B. Hutchings and R. Iannuzzelli, 'Taking a measure of fluid dynamics software', *Mech. Eng.*, **109**, 72–76 (May 1987).
16. B. Hutchings and R. Iannuzzelli, 'Benchmark problems for fluid dynamics codes', *Mech. Eng.*, **109**, 54–57 (June 1987).
17. R. Iannuzzelli and B. Hutchings, 'Fluid dynamics software gets down to work', *Mech. Eng.*, **109**, 60–63 (July 1987).
18. M. Engleman, *FIDAP: Users and Theoretical Manuals*, Fluid Dynamics International, Evanston, Ill., 1987.
19. P. M. Gresho and R. L. Lee, 'Don't suppress the wiggles—they're telling you something!' *Comput. Fluids*, **9**, 223–255 (June 1981).
20. H. S. Heaton, W. C. Reynolds and W. C. Kays, 'Heat transfer in passages, simultaneous development of velocity and temperature fields', *Int. J. Heat Mass Transfer* **7**, 763–781 (1964)
21. R. A. Wirtz and P. Dykshoorn, 'Heat transfer from arrays of flat packs in a channel flow', *Proc. 4th Int. Electronic Packaging Society Conf.*, October 1984, pp. 318–326.